# 6. Analysis of the transport phenomena

The universal transport abilities and the aggregation phenomenon appeared to be independent of the core type and most likely depend on the amphiphilic character of the shell. All synthesized and tested core-multishell architectures with PEI, PG-amine, and PAMAM core revealed similar encapsulation properties. For all of them the polymer self-aggregation was observed to play a crucial role for the transport behavior. Therefore the understanding of the nature of the aggregation phenomenon becomes very important for the further development and improvement of liposome-like polymers.

The aim of the experiments described in this paragraph was the determination of the aggregates size and their morphology. Also the interactions between guest molecules and the supramolecular structure were characterized. This included the guest encapsulation site (localization in the aggregate) and influence of the guest molecules on the behavior of the supramolecular aggregate. To complete this goal the following techniques have been applied:

1) molecular modeling
2) critical aggregation concentration (CAC) measurement by pendant drop method
3) dynamic light scattering (DLS)
4) cryo-transmission electron microscopy (CryoTEM)[409]
5) negative staining TEM
6) atomic force microscopy (AFM)

The polymer $PEI_{3600}(C_{18}mPEG_6)_{0.7}$ ($M_n$ = 18000 g mol$^{-1}$) was chosen as a standard polymer used for these experiments. The obtained results give a coherent model of the supramolecular aggregate as a novel type of vesicle with host-guest abilities.

## 6.1. Molecular modelling of core-multishell architecture

The molecular modelling of the unimolecular dendritic core-multishell architecture was performed with the program HyperChem release 6.0. A virtual model of $PEI_{3600}(C_{18}mPEG_6)_{0.7}$ containing ~ 3000 atoms was created. The molecules geometry was first optimized by the Fletcher-Reeves[410] (conjugate gradient) method and then by molecular dynamic computation in vacuo (for details see chapter 10.1.2). The obtained model possessed a diameter of 4.5 – 5 nm. Simulation in vacuo leads to highly compressed models due to the very (unnaturally) strong influences of Van der Waals forces. Therefore, computations in a periodic box filled with water molecules were performed. The molecular dynamic calculations resulted in a $PEI_{3600}(C_{18}mPEG_6)_{0.7}$ model with a diameter of 5.5 – 6.5 nm (Figure 48). In comparison to the calculation in vacuo, the molecule calculated in the periodic box revealed

approximately 2 nm bigger diameter. This was due to extension of the mPEG chains into the surrounding aqueous environment. Also a swelling of the polymer core was observed.

The obtained $PEI_{3600}(C_{18}mPEG_6)_{0.7}$ model with a diameter of approximately 6 nm was compared to the sizes measured by TEM and AFM and shown to have good conformity. For a better distinguishing between aggregated and nonaggregated polymers, single polymer will be refer to as "unimer" in the following chapters.
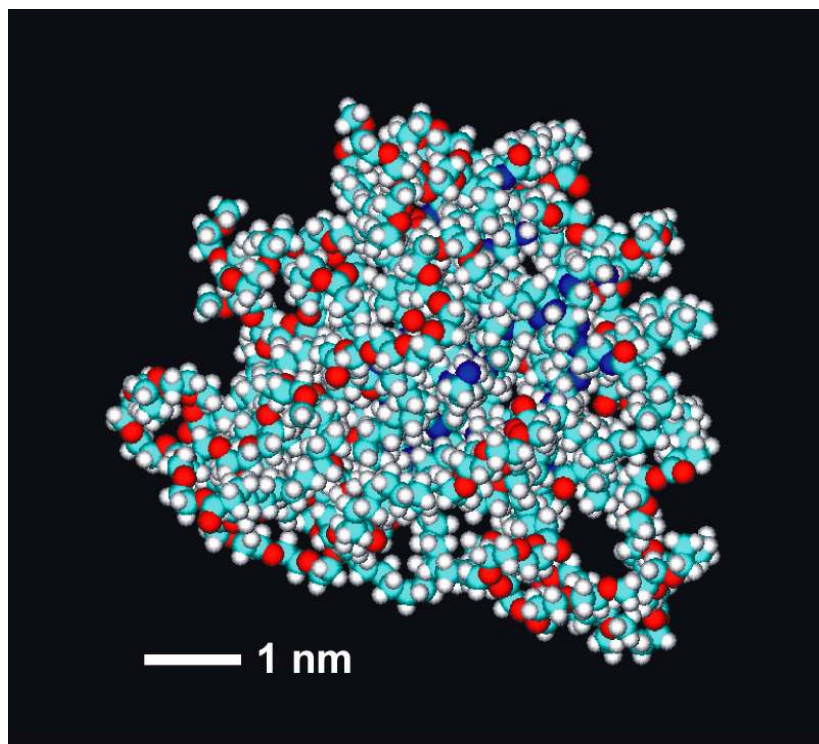


**Figure 48.** Molecular modeling of the unimolecular dendritic multishell architecture $[PEI_{3600}(C_{18}mPEG_6)_{0.7}]$ with HyperChem release 6.0. The "unimer" size is approximately 6 nm in diameter. Calculations were performed in a periodic water box.

## 6.2. CAC measurement for various core-multishell architectures

The critical aggregation concentration (CAC) was determined by the pendant drop method (experimental details see chapter 10.2.1.).[411] In this method, the surface tension of a liquid is extracted from the shape of a pendant drop which is formed at the tip of a capillary. The profile of the drop depends on the balance between gravity and surface forces. The equation of Bashforth and Adams which is based on Laplace's equation, relates the drop profile to the surface or interfacial tension through a nonlinear differential equation. The Gauss-Laplace equation represents a relationship between the curvature of a liquid meniscus and the surface tension $\gamma$ (Equation 10). In this equation $R_1$ and $R_2$ are the main radii of the curvature, $\Delta P_0$ is the pressure difference in a reference plane, $\Delta \rho$ is the density difference,

g is the acceleration due to gravity, and h is the vertical height of the drop measured from the reference plane.

$$\gamma \left( \frac{1}{R_1} + \frac{1}{R_2} \right) = \Delta P_0 + \Delta \rho g h$$

<div align="right">Equation 10</div>

The surface tension $\gamma$ can be determined by fitting the Gauss-Laplace equation to the coordinates of a drop, using $\gamma$ as the fitting parameter. By changing the $\gamma$ value a family of theoretical curves is obtained. The curve that fits best to the experimental points corresponds to the optimum value of the surface tension.[412]

Surface tension measurements were carried out over a wide range of concentrations for nanotransporters in aqueous solution in order to obtain information on the surface activity and critical aggregation concentration (CAC).

The surface tension-polymer concentration dependency experiment for $PEI_{3600}(C_{18}mPEG_6)_{0.7}$ is shown in Figure 49 as an example (congo red encapsulation-polymer concentration data are added for a better visualization of the aggregation-transport dependency). As can be seen in the graph, the surface tension decreases linearly with the logarithm of the polymer concentration according to the Gibbs adsorption isotherm, i.e., an usual behavior of surface-active compounds. At a characteristic concentration, there is a clear inflection point above which the surface tension remains almost constant. This trend implies that the dendritic multishell architectures in this respect behave like amphiphilic compounds. Therefore, in analogy to the critical micelle concentration (CMC) of surfactant solutions the aggregation of the unimers in the solution was confirmed. In case of $PEI_{3600}(C_{18}mPEG_6)_{0.7}$ the CAC was determined to be $6.5 \times 10^{-6}$ M (0.12 g $l^{-1}$) at 25 °C. All obtained CAC results are summarized in Table 13. All tested polymers revealed very low critical concentrations in the range of $10^{-8}$ to $10^{-6}$ M. The values are significantly lower than the CMC of typical ionic surfactants, such as potassium octadecanolate (CMC = $4.0 \times 10^{-4}$ M),[413] or non-ionic surfactants, such as alkyl-mPEGs (CMC range of $10^{-3}$ to $10^{-5}$ M),[414] and block copolymers, such as pluronics (PPO-b-mPEG; CMC range of $10^{-4}$ to $10^{-6}$).[193,415] The very low CAC values indicates a very good stability of the aggregates which was confirmed by size exclusion chromatography (SEC) of $PEI_{3600}(C_{18}mPEG_6)_{0.7}$ with encapsulated congo red on Sephadex LH-20 (insert in Figure 49).

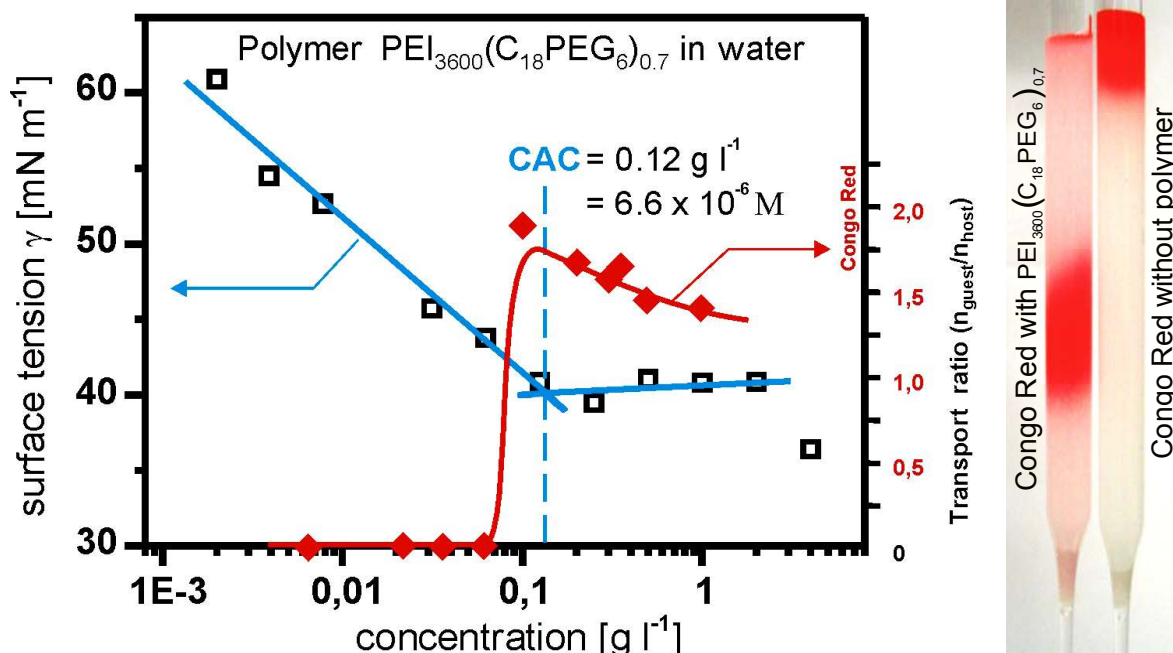**Figure 49.** Surface tension as a function of the concentration for the standard multishell nanotransporter $PEI_{3600}(C_{18}mPEG_6)_{0.7}$ ($\square$, left scale). The data allowed an estimation of the CAC value = 0.12 g l$^{-1}$; 6.6 $\times$ 10$^{-6}$ M. The transport capacity-concentration dependence for congo red ($\blacklozenge$, right scale) in chloroform is plotted for a better visualization of the encapsulation process. Insert on the right presents the SEC of the aggregates with encapsulated congo red in water.

**Table 13.** Critical aggregation concentrations of core-multishell polymers obtained by the pendant drop method in aqueous solution.

| Polymer | $M_n$ [g mol$^{-1}$] | CAC [mol l$^{-1}$] | CAC [g l$^{-1}$] |
|---|---|---|---|
| $PEI_{3600}(C_{12}mPEG_6)_{0.9}$ | 19000 | $1.2 \times 10^{-6}$ M | 0.023 |
| $PEI_{10500}(C_{12}mPEG_6)_{0.9}$ | 48000 | $5.6 \times 10^{-7}$ M | 0.027 |
| $PEI_{3600}(C_{18}mPEG_6)_{0.7}$ | 18000 | $6.6 \times 10^{-6}$ M | 0.120 |
| $PEI_{3600}(C_{18}mPEG_6)_{0.9}$ | 22000 | $8.0 \times 10^{-7}$ M | 0.018 |
| $PEI_{3600}(C_{18}mPEG_6)_{1.0}$ | 24000 | $7.3 \times 10^{-7}$ M | 0.018 |
| $PEI_{3600}(C_{18}mPEG_{14})_{0.7}$ | 27000 | $1.8 \times 10^{-7}$ M | 0.005 |
| $PEI_{10500}(C_{18}mPEG_6)_{0.7}$ | 44000 | $4.3 \times 10^{-7}$ M | 0.019 |
| $PEI_{10500}(C_{18}mPEG_{10})_{0.7}$ | 55000 | $5.6 \times 10^{-8}$ M | 0.003 |
| $PEI_{10500}(C_{18}mPEG_6)_{0.9}$ | 53000 | $1.7 \times 10^{-7}$ M | 0.009 |

Surface tension measurements have shown that changes of the core size from $PEI_{3600}$ to $PEI_{10500}$ (both with $(C_{18}mPEG_6)_{0.9}$ shells) cause a significant decrease of the CAC from $8.0 \times 10^{-7}$ M to $1.7 \times 10^{-7}$ M. For polymers with the $(C_{18}mPEG_6)_{0.7}$ shell the CAC changed with increasing core size from $6.6 \times 10^{-6}$ M to $4.3 \times 10^{-7}$ M. By a modification of the alkyl chain length from $C_{12}$ to $C_{18}$ a slight decrease of the CAC was observed for both core sizes: for $PEI_{3600}(C_{12}mPEG_6)_{0.9}$ and $PEI_{3600}(C_{18}mPEG_6)_{0.9}$ from CAC $= 1.2 \times 10^{-6}$ M to $8.0 \times 10^{-7}$ M and for $PEI_{10500}(C_{12}mPEG_6)_{0.9}$ and $PEI_{10500}(C_{18}mPEG_6)_{0.9}$ from CAC $= 5.6 \times 10^{-7}$ M to CAC $= 1.7 \times 10^{-7}$ M. Changes of the functionalization level from 70% to 90% and 100 % cause a decrease of the CAC value from $6.5 \times 10^{-6}$ M to $8.0 \times 10^{-7}$ M and $7.3 \times 10^{-7}$ M for $PEI_{3600}(C_{18}mPEG_6)_x$. With the prolongation of the mPEG chains the CAC of polymers dropped from $8.0 \times 10^{-7}$ M for $PEI_{3600}(C_{18}mPEG_6)_{0.9}$ to $1.8 \times 10^{-7}$ M for $PEI_{3600}(C_{18}mPEG_{14})_{0.9}$. To summarize, an increase of the core size, alkyl chain length, mPEG chain length, and degree of functionalization decreases the nanotransporters CAC.

CAC values observed for core-multishell architectures range from 0.003 to 0.120 g $l^{-1}$ ($5.6 \times 10^{-8}$ M to $6.6 \times 10^{-6}$ M). However, the aggregation phenomena observed for congo red encapsulation occurred in the concentration range of 0.05 to 0.20 g $l^{-1}$. The presence of the polymer in solution after filtration of the samples with concentration below the CAC was confirmed by $^1$H NMR. Therefore the CAC has to be influenced by an additional, external factor, not only by the nanotransporters chemical composition.

The influence of the guest molecules on the critical aggregation concentration was determined by using of nimodipine and β-carotene. Differences between the CAC of the pure $PEI_{3600}(C_{18}mPEG_6)_{0.7}$ solution and with encapsulated guest molecules were observed. The encapsulation of nimodipine changed the CAC from $6.6 \times 10^{-6}$ M to $5.0 \times 10^{-6}$ M (from 0.12 to 0.90 g $l^{-1}$). β-carotene encapsulation increased the CAC from $6.5 \times 10^{-6}$ M to $1.5 \times 10^{-5}$ M (0.27 g $l^{-1}$). Surprisingly, the CAC for congo red loaded polymers (CAC $= 0.24$ g $l^{-1}$; $1.3 \times 10^{-5}$ M) was similar to the CAC obtained for nanotransporters with β-carotene. The encapsulation of vitamin $B_6$ decreased the critical aggregation concentration (CAC $= 4.1 \times 10^{-6}$ M) similar to encapsulation of nimodipine. This results indicate that the guest molecules act as cosurfactants for the aggregate and shift the the CAC of the guest-host complexes. Additionally important is that the change of the critical concentration is dependent not on the guests' polarity but on the molecules' geometry. This observation was also confirmed by DLS and CryoTEM measurements.

## 6.3. Dynamic light scattering measurements of polymers

In the DLS experiments, the intensity-time correlation function $g_2(\tau)$ was measured. The hydrodynamic radius was extracted from these measurements by a second-order cumulants'

fitting of $g_2(\tau)$. The hydrodynamic radius $R_h$ can be obtained from the Stokes-Einstein equation (Equation 11) where $k_B$ is the Boltzmann's constant, $T$ is the absolute temperature, $\eta$ is the coefficient of viscosity of the solvent, and $D_0$ is the translation diffusion coefficient calculated from $g_2(\tau)$ (for more information see chapter 10.1.2.).[416-418]

$$\langle R_h \rangle = \frac{k_B T}{6\pi\eta D_0} \qquad\qquad \text{(Equation 11)}$$

DLS measurements were performed in a polymer concentration range from 0.002 to 10.0 g l$^{-1}$ at the wavelength of 620 nm at 25 °C. However, the scattering intensity below the CAC was very low, which led to an unfavorable signal-to-noise ratio and resulted in unreliable scattering data. Therefore, only the data above the CAC were used in the discussion.

The data analysis by the cumulant fitting model (particle mono distribution model) led to low correlation values between the experimental points and the mathematical model. Therefore a bi-exponential fitting model was chosen for analysis. Results were additionally confirmed by correlation with the Laplace inversion fitting method which led as well to a bi-distribution of the diameters. This suggests the presence of two different particles sizes in the polymer solution.

Dynamic light scattering measurements performed in water for $PEI_{3600}(C_{18}mPEG_6)_{0.7}$ revealed the presence of particles with two different diameters (Figure 50) – "unimers" (nonaggregated nanotransporters) and supramolecular aggregates. The smaller species – "unimers" – possessed the diameters of approximately 3.1 nm calculated by Laplace inversion and 4.5 nm obtained with the bi-exponential fitting. This was in good agreement with the particle size obtained from molecular modelling. The bigger particles – aggregates – had diameters of 34.9 (Laplace inversion fitting) or 34.6 nm (bi-exponential fitting). By comparison of the volumes of "unimer" (~ 5 nm) and aggregate (~ 34.7 nm) the average number of polymers per aggregate can be calculated by assuming a cubic or hexagonal close packing configuration (Equation 12).

$$0.74 \times \left( \frac{4\pi}{3} R_{agg}^3 \right) = N \times \left( \frac{4\pi}{3} R_{unimer}^3 \right) \qquad\qquad \text{(Equation 12)}$$

$$N = 0.74 \times \frac{R_{agg}^3}{R_{unimer}^3}$$

$R_{agg}$ is the radius of the aggregate, $R_{unimer}$ is the radius of the "unimer", and $N$ is the number of unimers creating the aggregate. The total number of approximately 250 core-multishell architectures per aggregate was obtained.
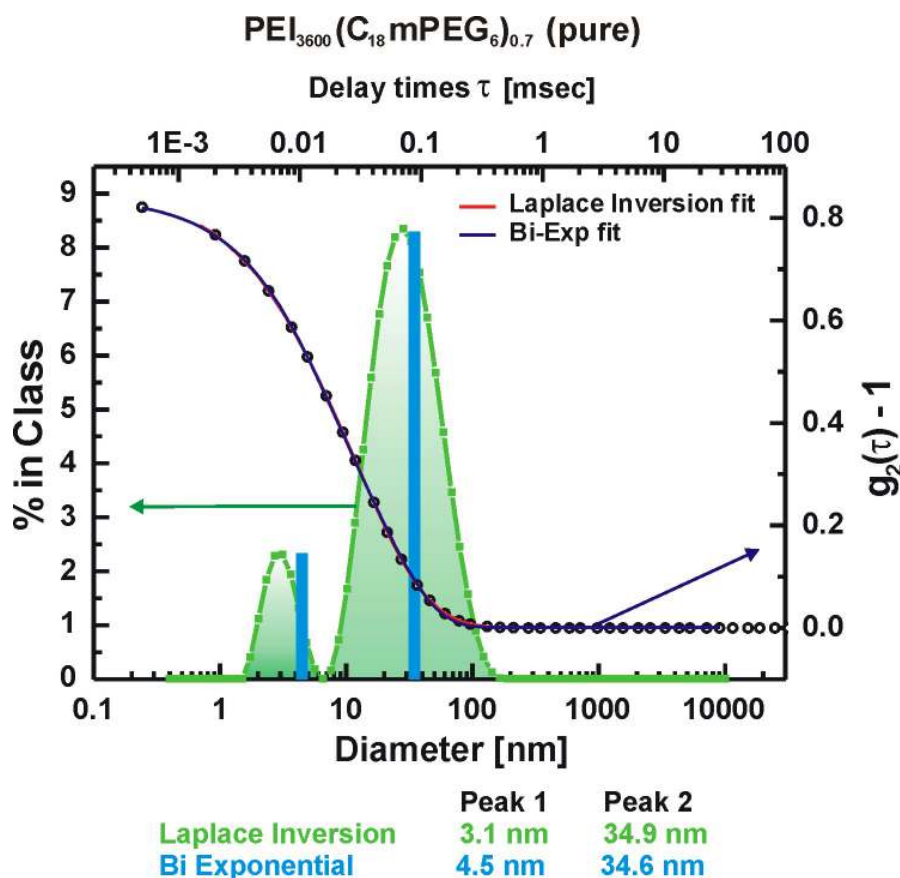


**PEI$_{3600}$(C$_{18}$mPEG$_6$)$_{0.7}$ (pure)**

| | Peak 1 | Peak 2 |
|---|---|---|
| **Laplace Inversion** | 3.1 nm | 34.9 nm |
| **Bi Exponential** | 4.5 nm | 34.6 nm |

**Figure 50.** Particle sizes obtained by dynamic light scattering with Laplace inversion fitting (green) and bi-exponential fitting (blue) for pure PEI$_{3600}$(C$_{18}$mPEG$_6$)$_{0.7}$ in water. Additionally the correlation function data (**o**) and fittings: Laplace (**–**) and bi-exponential (**–**) are shown.

The scattering intensity in chloroform was smaller than in water. This is due to the fact that the refractive index of PEG (1.453) is very close to the one of chloroform (1.4459; matching solvent condition). Therefore, PEG chains become invisible in chloroform, which results in the observation of a slightly smaller (~30 nm) size of the aggregates in chloroform.

After the encapsulation of guest molecules a drastic change of the aggregates diameter was observed. Surprisingly, although consistent with observation from the CAC measurement, the changes of the diameter of the aggregates did not depend on the guest molecules polarity but on the geometry of the molecules.

With the encapsulation of compact molecules like nimodipine in water (Figure 51) or vitamin B$_6$ in chloroform a decrease of the aggregates diameter was detected for PEI$_{3600}$(C$_{18}$mPEG$_6$)$_{0.7}$. The new diameter in water was 21.9 (Laplace Inversion) or 23.2

*Michał R. Radowski, Dissertation*

(bi-exponiential) nm for $PEI_{3600}(C_{18}mPEG_6)_{0.7}$ with nimodipine. For the polymer with vitamin $B_6$ in chloroform the aggregates' size was approximately 19.0 – 20.0 nm. Also in this case the unimers were detected in the solution with the size of 3.0 – 3.5 nm. The average number of unimers per aggregate calculated form equation 12 was 150.
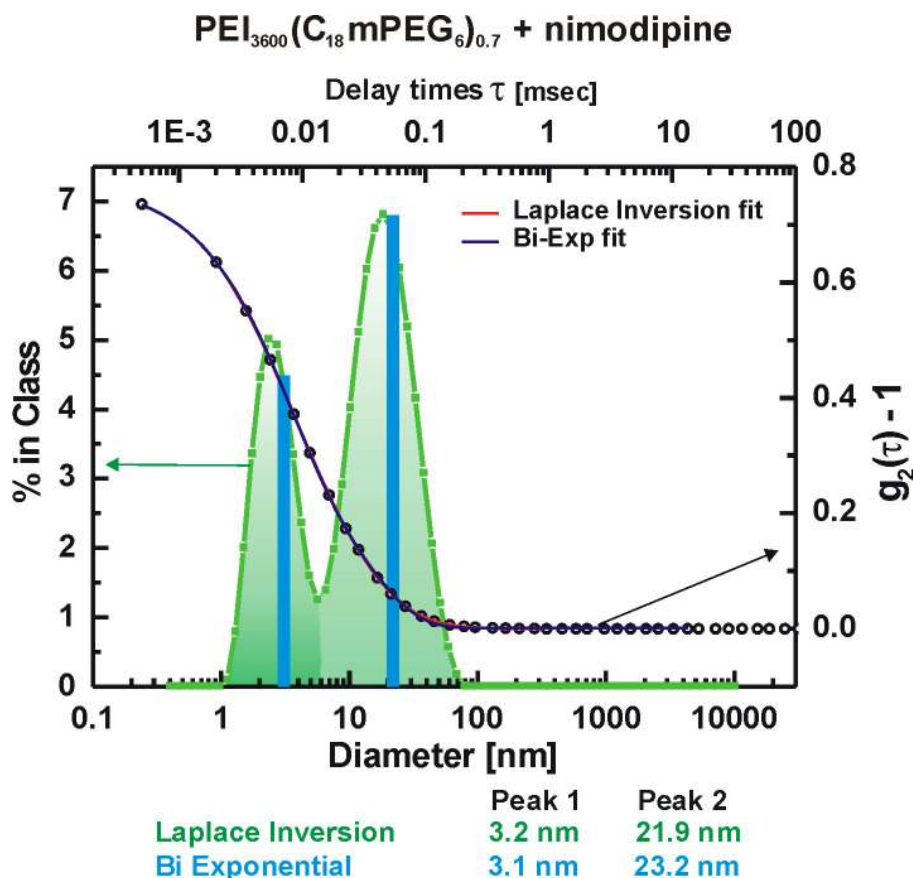


**Figure 51.** Particle sizes obtained by dynamic light scattering with Laplace inversion fitting (green) and bi-exponential fitting (blue) for $PEI_{3600}(C_{18}mPEG_6)_{0.7}$ with encapsulated nimodipine in water. Additionally the correlation function data (**o**) and fittings: Laplace (**–**) and bi-exponential (**–**) are shown.

With the encapsulation of linear guest molecules like β-carotene in water (Figure 52a) or congo red in chloroform (Figure 52b) an increase of the aggregates size was observed. The aggregate diameter grew from 34 nm (pure polymer) to 120 – 140 nm with encapsulated β-carotene, and to 120 – 150 nm for polymers with congo red. It is noteworthy that no small particles (unimers) were detected. This was due to the fact that large particles scatter much more light than small particles. The scattering intensity of a particle is proportional to the sixth power of its diameter. If a sample contains two sizes of particles of 5 nm and 150 nm with an equal number for each particle size, then the scattering intensity ratio will be $1 : 7.29 \times 10^8$ (!). Therefore, smaller particles will not be seen with the DLS technique. Calculations (equation 12) showed that one aggregate consists of approximately 20000 (!) unimers.

*Michał R. Radowski, Dissertation*

Surprisingly the polarity of the solvent and the polarity of the guest molecules had no influence on the aggregates' size. The dimension of the supramolecular species depended only on the geometry of the guests – compact or linear. This may be due to the fact that these compact molecules are preferentially located in the interfacial region and behave as co-surfactants by reducing interfacial tension and thus decrease the size and CAC. The linear molecules might act as linkers between the unimers (bridging units) and therefore can stabilize bigger aggregates. Thus the CAC would increased. This guest molecule-aggregate size dependency was also observed for the polymer with other cores than PEI. For nanotransporters with PG-amine or PAMAM core and encapsulated congo red DLS measurement revealed aggregates with diameters between 150 and 200 nm.

Modification of the core size of the polymer from $PEI_{3600}$ to $PEI_{10500}$ resulted in an increase of the aggregates size in both water and chloroform from ~ 30 nm to ~ 60 nm. After the encapsulation of guest molecules, similar trends for the changes of the size were observed. The incorporation of nimodipine decreased the aggregate diameter to ~ 25 – 30 nm, while the uptake of congo red increased the aggregate size to ~ 130 – 150 nm. Modification of the outer shell size, the inner shell size, and the degree of functionalizatoion did not significantly influence the aggregates size. Thus all described interactions between nanotransporters and guest molecules were independent of the polymer structural.
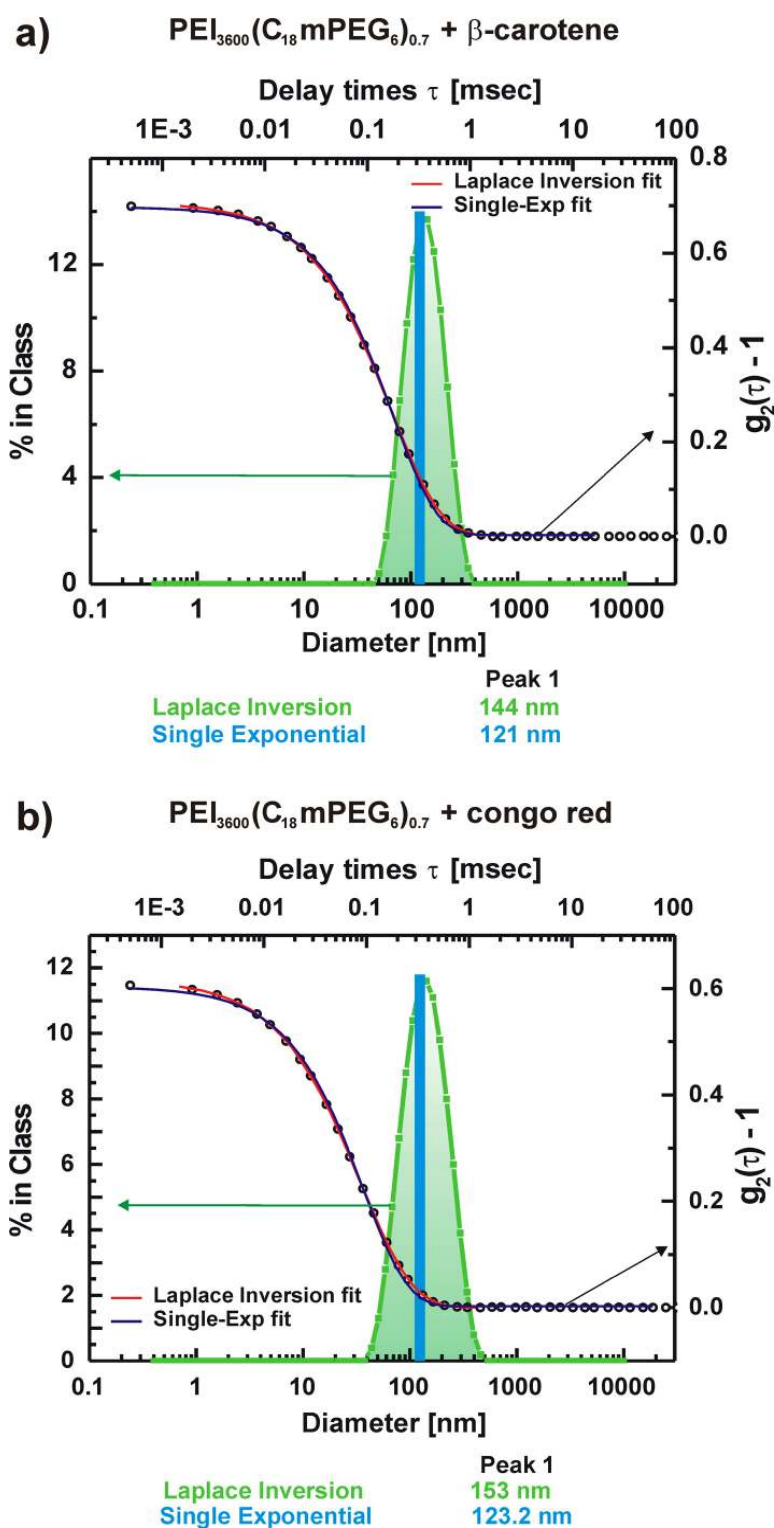
**Figure 52.** Particle sizes obtained by dynamic light scattering with Laplace inversion fitting (green) and bi-exponential fitting (blue) for $PEI_{3600}(C_{18}mPEG_6)_{0.7}$ with encapsulated (a) $\beta$-carotene in water and (b) congo red in chloroform. Additionally the correlation function data (**o**) and fittings: Laplace (**−**) and bi-exponential (**−**) are shown.

*Michał R. Radowski, Dissertation*

## 6.4. CryoTEM measurements of the polymers

The direct structural analysis of the aggregates detected by DLS (and indirectly by CACs and encapsulation measurements) was performed by CryoTEM[409] measurements with $PEI_{3600}(C_{18}mPEG_6)_{0.7}$ in the concentration range from 0.01 to 1.0 g l$^{-1}$. This technique was chosen due to the lack of interactions between unimers (and aggregates) and the surface or other external factors which was the case for AFM measurements, see chapter 6.6. Therefore the undisturbed aggregates in the solution could be observed. These measurements can only be performed in aqueous media (chloroform cannot be used as a solvent). Samples of pure $PEI_{3600}(C_{18}mPEG_6)_{0.7}$, polymer loaded with nimodipine, and polymer with encapsulated β-carotene were tested. This allowed confirmatio of the dependence of the aggregates size observed by DLS and analysis of the supramolecular internal structure.

The CryoTEM micrographs revealed two coexisting types of objects for the dendritic core-multishell architectures in water when the concentration of the polymer was similar or higher to CAC. At concentrations below the aggregation point, no supramolecular structures were observed (Figure 53).
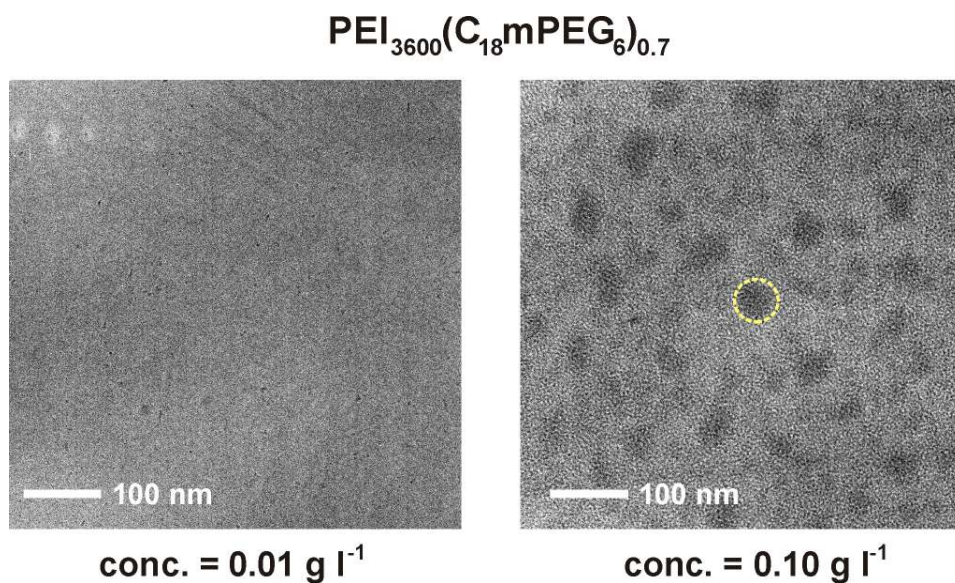


$$PEI_{3600}(C_{18}mPEG_6)_{0.7}$$

conc. = 0.01 g l$^{-1}$      conc. = 0.10 g l$^{-1}$

**Figure 53.** CryoTEM micrographs of $PEI_{3600}(C_{18}mPEG_6)_{0.7}$ in water at a polymer concentration of 0.01 g l$^{-1}$ ($5.5 \times 10^{-7}$ M) (left) and 0.10 g l$^{-1}$ ($5.5 \times 10^{-6}$ M) (right). Samples with a concentration below the CAC value showed no visible aggregation phenomenon, while supramolecular aggregates were observed at the concentration close to the CAC = $6.6 \times 10^{-6}$ M (single aggregate is marked on the picture with a yellow circle).

The diameters of the aggregates for pure polymer were between 30 and 50 nm. The small nanoparticles – unimers possessed the diameter of 4 – 6 nm (Figure 54). Both results

were in the good agreement with the particle sizes obtained from DLS measurements. It was noteworthy that the micrographs revealed a noticeably granular fine structure and very high contrast of the aggregates. The ultrastructural features were fundamentally different from the CryoTEM images of liposomes and micelles.[419] This proved that aggregates were densely packed species formed by a large number of the "elementary" polymers (unimers). Interestingly, in the areas where unimers are densely packed the typical interparticle spacing between the centers of the polymers did not fall below 8 – 9 nm. This finding was an indirect indication that an outer shell of the particles, which was not visible in the images, prevents a denser packing.
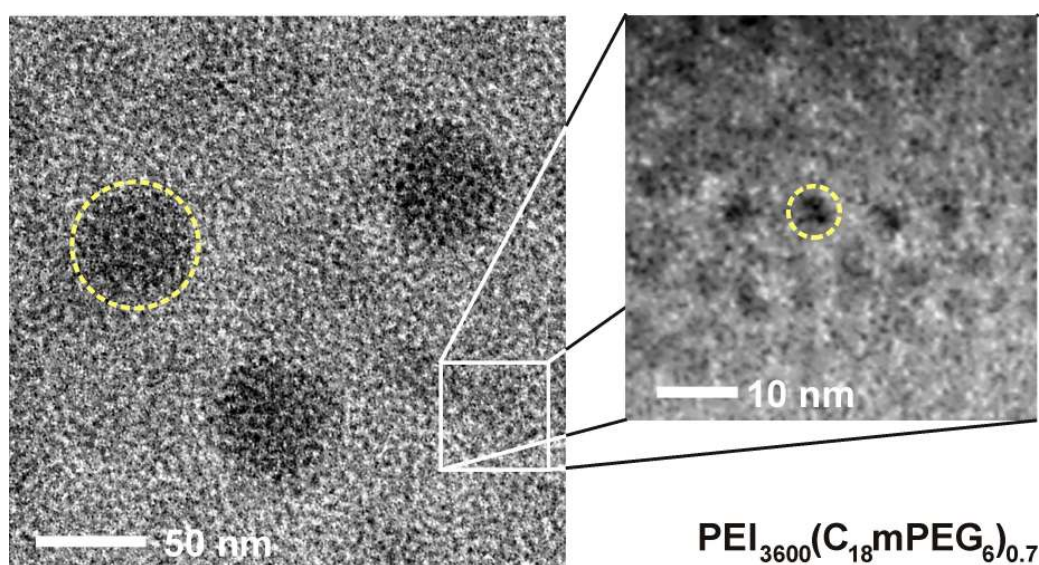


**Figure 54.** Micrographs of $PEI_{3600}(C_{18}mPEG_6)_{0.7}$ aggregates (left) and unimers (right) in water at the concentration of 0.10 g $l^{-1}$ (5.5 × $10^{-6}$ M). The diameters of the aggregates were in the range of 30 to 50 nm and the diameters of the single polymers were between 4 to 6 nm. Due to the electron density only the polyamine core can be seen on the micrographs as black dots.

After the encapsulation of nimodipine in $PEI_{3600}(C_{18}mPEG_6)_{0.7}$ the CryoTEM experiments revealed smaller aggregates than observed for the pure polymer (Figure 55, left micrograph). A typical assembly size lay in the range of 25 to 35 nm and the contrast on the micrographs was significantly lower. With the incorporation of β-carotene the aggregate size dramatically increased to the diameter of 120 to 140 nm (Figure 55, right micrograph). Also the contrast of the micrographs increased significantly. In both samples small particles – unimers – were visible with the size of 4 to 6 nm.

These experiments fully confirmed the guest molecule geometry – size aggregate dependency observed by dynamic light scattering.
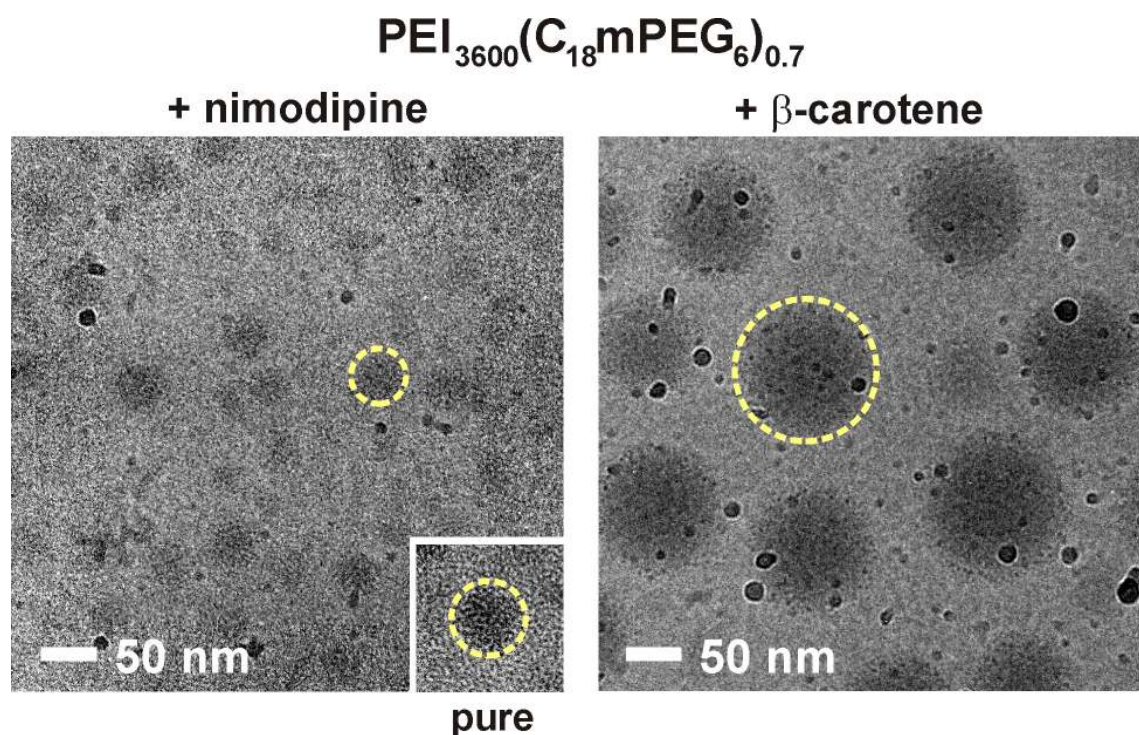
$$PEI_{3600}(C_{18}mPEG_6)_{0.7}$$



**Figure 55.** Micrographs of $PEI_{3600}(C_{18}mPEG_6)_{0.7}$ with encapsulated nimodipine (left) and with encapsulated β-carotene (right) in water at the concentration of 1.00 g $l^{-1}$ (5.5 × $10^{-5}$ M). The aggregates diameters with nimodipine were 25 to 35 nm. Assemblies with β-carotene revealed diameters of 120 to 140 nm. For comparison, the aggregate of pure polymer is shown in the insert with identical scale.

## 6.5. Negative staining TEM

The spacing of 8 – 9 nm between centers of the unimers at densely packed areas observed in the CryoTEM were assumed to be filled with outer shell chains which prevent a closer packing. To prove this theory the supramolecular aggregates were embedded in a matrix of heavy metal salt (uranyl acetate), as is usually done for high contrast imaging in TEM. In the obtained picture the total diameter of the particles became visible (including outer shell) and were in the expected value of 8 to 9 nm (Figure 56).
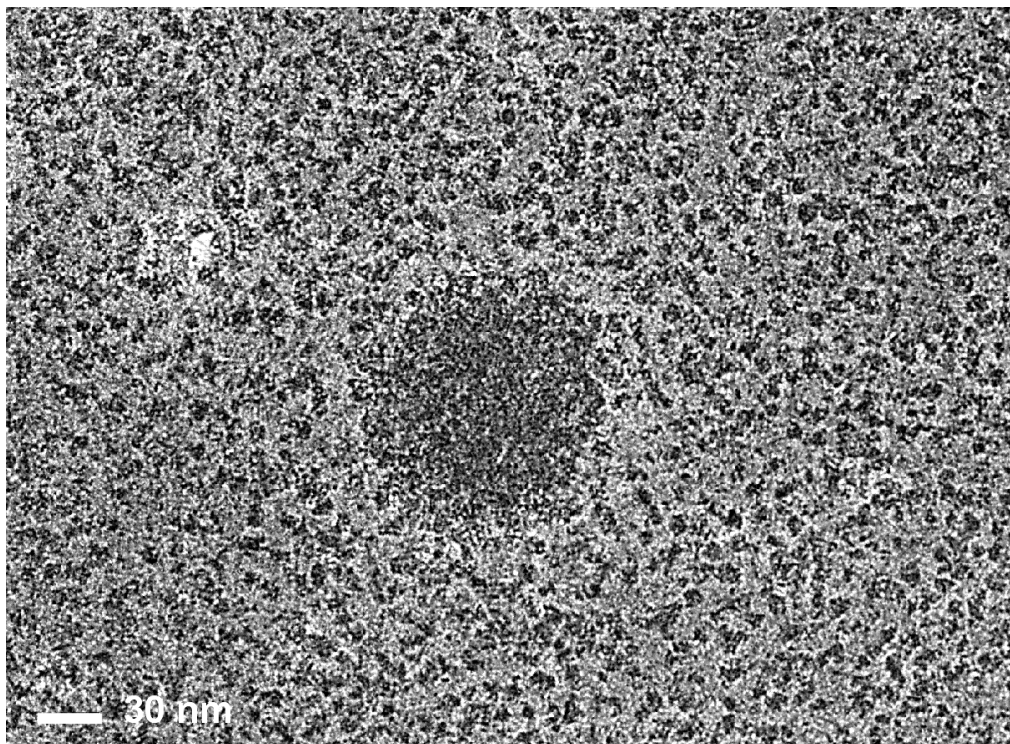
*Michał R. Radowski, Dissertation*

**Figure 56.** TEM micrograph (the contrast has not been inverted for better visibility) of pure $PEI_{3600}(C_{18}mPEG_6)_{0.7}$, which was deposited and dried on a carbon film after staining with uranyl acetate (1 % w/v) . The image shows monomolecular species with a typical size of 8 - 9 nm and one large aggregate. To permit the imaging of isolated particles the polymer solution (of 1.0 g/L) was diluted to 0.01 g/L prior to sample preparation.

## 6.6. AFM measurements of the polymers

$PEI_{3600}(C_{18}mPEG_6)_{0.7}$ was measured by AFM on mica and HOPG (highly ordered pyrolytic graphite) with the tapping mode (intermittent contact mode) experiment (for details see chapter 10.2.1.). Mica is used as a standard background material for AFM with a regular lattice structure with polar surface, negatively charged in water. The HOPG is a relatively new form of high purity carbon. Unlike mica, HOPG is completely non-polar and provides a background with only carbon in the elemental signature. Therefore both measurements were performed in order to obtain structures with two different interactions between polymer and surface.

The experiments with pure nanotransporters exposed on mica revealed randomly ordered rod- or hook-like assemblies of 4 to 10 polymers with the assumption of the unimers' diameter of 5 to 6 nm. Occasionally long fibers were observed with apparent interruptions at high magnification. No ordering effect of mica on the polymer was observed, although the height of the monomers was three times smaller than predicted from previous experiments and polymer modelling. This was probably due to strong interactions between the core-

multishell architectures and the mica surface that led to flattening of the polymer (enamel formation).

The same preparation on HOPG resulted in a much better organized molecular assembly of $PEI_{3600}(C_{18}mPEG_6)_{0.7}$. Nanotransporters similar to the ones on mica created rows of 4 to 10 molecules. However, the in case of the HOPG the surface polymers were strictly ordered along the crystal axes of the graphite at an angle of about 60°. The distance between the molecules was evaluated to 7 – 8 nm with the height of the unimers (single polymers) of 4 to 5 nm. The column-to-column distance was 7 to 8 nm (Figure 57).
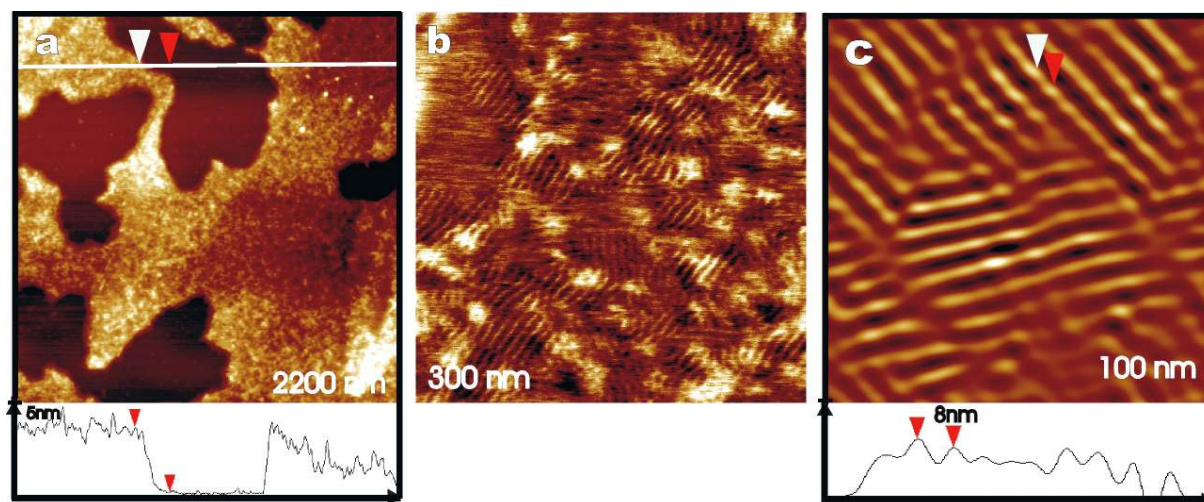


**Figure 57.** AFM images of $PEI_{3600}(C_{18}mPEG_6)_{0.7}$ on HOPG (a, b) with different resolutions and c) high-resolution image of S1 columns.

AFM measurements (on HOPG) of $PEI_{3600}(C_{18}mPEG_6)_{0.7}$ with encapsulated congo red as a guest molecule revealed a ordered pattern similar to the one obtained for the pure sample. However, a large number of cross links was observed in the previously empty spaces between the polymer rows. The high resolution micrographs produced frequent hexagonal patterns. The height of 5 nm was measured for fibers and 7 - 8 nm for hexagonal patterns (Figure 58). This indicates that congo red acts as a linking (bridging) molecule. An excess of the dye is orientated vertically to the HOPG surface and stick out from polymeric particles. The distance between columns was 7.0 to 7.2 nm and distance between cross-linked congo red was 14 – 15 nm.
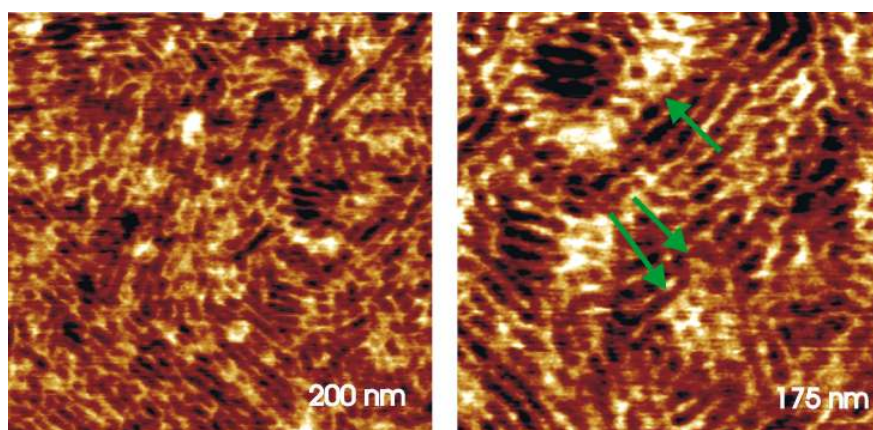
**Figure 58.** AFM images of the interaction between $PEI_{3600}(C_{18}mPEG_6)_{0.7}$ and congo red on HOPG. Hexagonal patterns are marked with arrows.

The encapsulation of nimodipine in $PEI_{3600}(C_{18}mPEG_6)_{0.7}$ caused the changes in the pattern observed by AFM on HOPG. This order was only observed in one direction with a particle height of 5 nm. The whole pattern was more disturbed than the one observed for the pure polymers or for nanotransporters with incorporated congo red. Similar to the dye molecules, nimodipine was located between the unimers. The distance between the columns was 17 nm and the distance between cross-linking nimodipine was 7 to 8 nm (Figure 59).
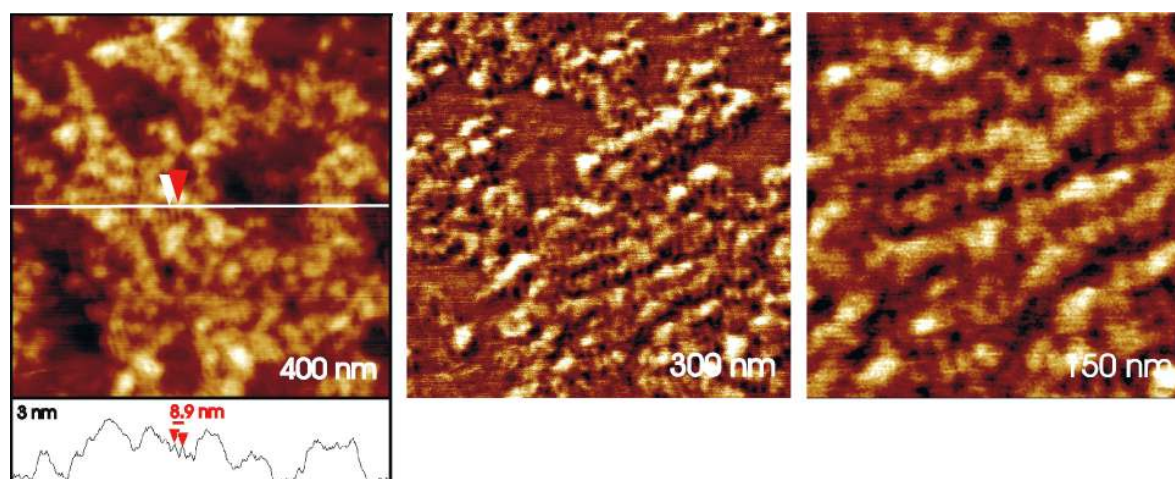


**Figure 59.** AFM images of the interaction between $PEI_{3600}(C_{18}mPEG_6)_{0.7}$ and nimodipine on HOPG.

To summarize, AFM experiments revealed the tendency of core-multishell architectures to create regular patterns on highly ordered pyrolytic graphite. The obtained pattern can be strongly influenced by the encapsulation of guest molecules. Linear molecules such as congo red stabilize the pattern and act as bridging units between the polymers. With the encapsulation of compact molecules like nimodipine the pattern was strongly disturbed. This was a confirmation for the observations from DLS and CryoTEM where linear molecules

*Michał R. Radowski, Dissertation*

creates larger aggregates and compact molecules decrease the diameter of the aggregates. Additionally, what is the most important, no encapsulation of guest molecules inside the polymer was detected (no size change of polymer was observed). All guests were exclusively encapsulated in the intermolecular spaces.

## 6.7. Discussion of the transport theory of supramolecular aggregates

The results presented above create the coherent model of a new type of encapsulation mechanism discovered for core-multishell architectures. All previously reported core-shell structures in the literature were characterized as unimolecular transporters (unimeric micelles, "dendritic box").[10,19,57,71-73,75,77,78,80,82,269,347,350-352,354,356,361,420-422] The aggregation of core-shell particles was observed,[23,349,350,361] but the host-guest abilities of the particles were never associated (connected) to an aggregation phenomenon. Although, enhancement of the transport capacity was explained as a possible core-shell unimolecular micelle association. [350,361]

Studies on the transport capacity-polymer concentration dependency performed for core-multishell architectures revealed the nonlinear behavior with a clear CAC (CMC) point, which is characteristic for block copolymers micelles. This type of transport was observed for all synthesized liposome-like polymers independent of their structural composition. However, the structure of the polymer influences the transport capacity in a quantitative manner.

To better understand the observed supramolecular aggregation phenomenon (clearly responsible for the host-guest interactions) the aggregate formation and its structural aspects were investigated by three independent and – what is important – non-invasive techniques: surface tension measurement, dynamic light scattering, and Cryo-TEM. The pure polymer, polymer with encapsulated compact guest molecules (nimodipine, vitamin $B_6$), and polymer with encapsulated linear molecules ($\beta$-carotene, congo red) were tested for all of them. The decrease of the surface tension with increasing polymer concentration was observed for all core-multishell architectures. This typical behavior for surface active molecules allowed to determine the critical aggregation concentration for all polymers. Thus it was concluded that lipisome-like nanotransporters act as (and are) amphiphilic compounds. The independently performed measurements for $PEI_{3600}(C_{18}mPEG_6)_{0.7}$ revealed the presence of the aggregates' state in solutions with the concentration of nanotransporters above the CAC value. No aggregates have been found in solutions with a concentration below the CAC. The size of the aggregates measured by DLS was around 35 nm in water and 25 – 30 nm in chloroform. This was due to the similar refractive index of mPEG and chloroform which causes the "invisibility" of the mPEG chains in the organic phase. The obtained values were confirmed by the direct observation of the supramolecular aggregates by CryoTEM. The micrographs revealed densely packed spheres (aggregates) with diameters ranging from 30 to 50 nm

(Table 15). It is very important that the observed structures possessed a significantly different structure compared to liposomes or micelles observed by the same technique.[419] Therefore the liposome or micelle creation can be excluded from further discussions.

**Table 14.** Summary of the unimer and aggregate sizes of $PEI_{3600}(C_{18}mPEG_6)_{0.7}$ obtained by molecular modelling (MM), DLS, TEM, and Cryo-TEM.

| $PEI_{3600}(C_{18}mPEG_6)_{0.7}$ | solvent | CAC $[g\ l^{-1}]$ | Aggregate [nm] | | Unimer [nm] | | |
|---|---|---|---|---|---|---|---|
| | | | DLS | Cryo-TEM | DLS | Cryo-TEM | MM / TEM |
| without guest | water | 0.12 | 30-35 | 30-50 | 3-4 | 4-5 | 5-6 / 8-9 |
| without guest | chloroform | - | 25-30 | - | 3-4 | - | - |
| + vitamin $B_6$ | chloroform | - | 20-25 | - | 3-5 | - | - |
| + nimodipine | water | 0.09 | 20-25 | 20-30 | 3-4 | 4-5 | - |
| + congo red | water | 0.24 | 130-160 | - | - | - | - |
| + congo red | chloroform | - | 130-150 | - | - | - | - |
| + β-carotene | water | - | 120-140 | 120-140 | - | 4-6 | - |

With the encapsulation of guest molecules, changes of the size of the aggregates were observed. These changes were independent of the polarity of the guest molecules and environment (solvent) but were dependent on the structure (geometry) of the guest molecules. The encapsulation of compact molecules caused the decrease of the aggregate diameter from 30 – 35 nm to only 20 – 25 nm which was observed by DLS and CryoTEM. No change of the aggregates' structure (packing) was notice. Additionally, a small change in the CAC was observed. With the incorporation of linear molecules an increase of the aggregates size from 30 – 35 nm to 120 – 160 nm was confirmed by both techniques. Also the CAC value increased from 0.12 to 0.24 g $l^{-1}$. It is noteworthy that all measurements revealed the presence of small particles next to the aggregates with the diameter of 3 to 6 nm (negative staining TEM = 8 – 9 nm), which corresponds to the size calculated by molecular modelling for the unimolecular $PEI_{3600}(C_{18}mPEG_6)_{0.7}$ nanotransporters.

The presence of unimers in the solutions in addition to the aggregates indicates that the aggregates are in a constant dynamic equilibrium that is shifted towards the aggregated state (Figure 60).
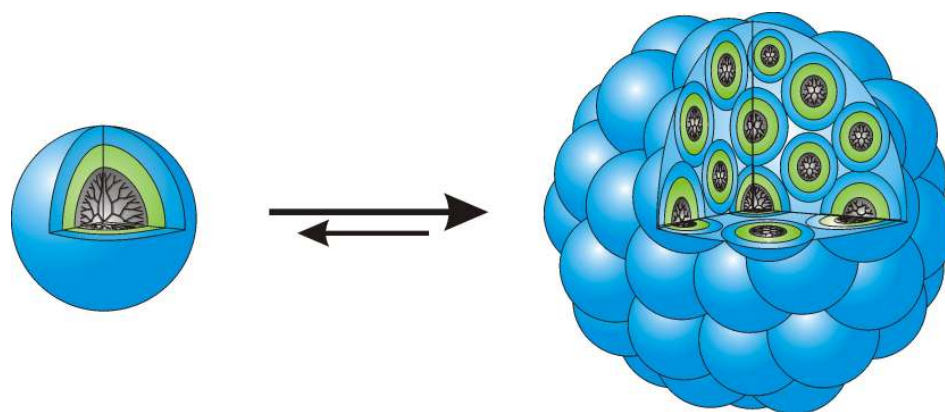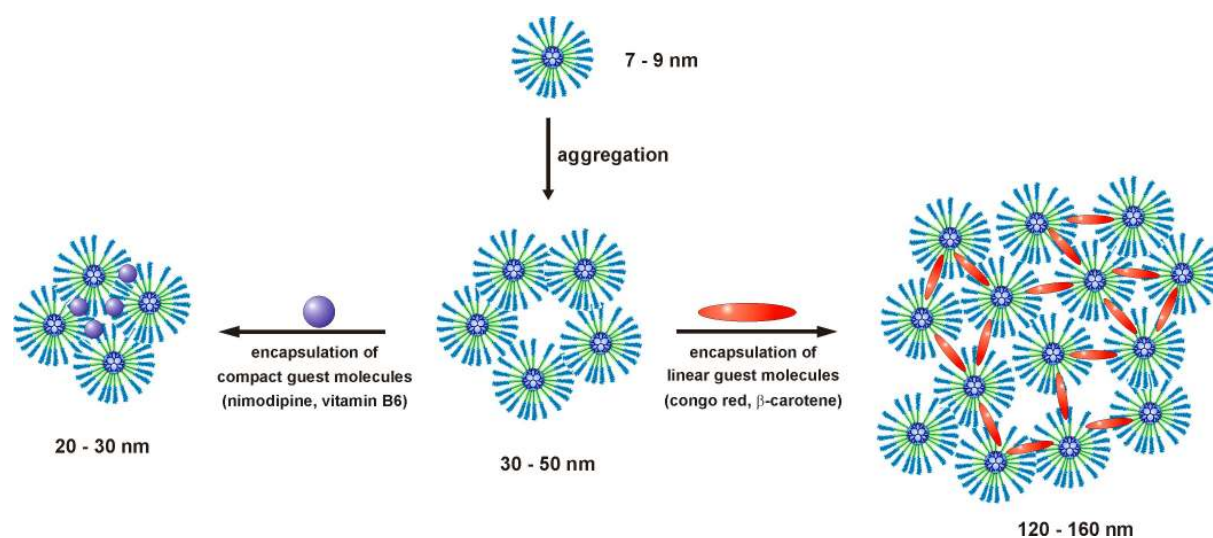
**Figure 60.** Graphical representation of the core-multishell architecture and supramolecular aggregates in the dynamic equilibrium in solution.

The mechanism which is responsible for the creation of the aggregates is probably similar to the formation of micelles. The presence of aliphatic chains in the polymeric structure leads to a close packing of the dendritic structure which minimizes the hydrophobic-hydrophilic contact surface area similar to di-block polymeric micelles.[235,237-239] Due to the spherical structure of the core-shell architectures (Figure 48) the creation of the micelles is thermodynamically unfavorable. Therefore, aggregate formation occurs where polymers are packed site by site to each other, hence reducing the contact surface area between environment and hydrophobic domains. The larger hydrophobic domains are, the more stable aggregates become. This can explain the high transport capacity for both polar and nonpolar guest molecules for polymers with $C_{18}$ chains while no or limited encapsulation abilities occur for core-shell architectures equipped with $C_0$, $C_6$, and $C_{12}$. Additionally to hydrophobic polymer-polymer interactions the presence of mPEG chains also stabilizes the aggregates by creation of a PEG network with hydrogen bonds as linking species.[350,372]

Self-aggregation and dynamic exchange between aggregates and unimers opens the question of the mechanism of encapsulation and localization of the guest molecules. The appearance of host-guest interactions only above the CAC together with changes of the CAC values and aggregates size influenced by guest molecules uptake clearly indicates that the encapsulation site cannot be located only inside the core-multishell structure. Small, compact molecules (nimodipine, vitamin $B_6$, nile red) are preferentially located in the interfacial region and behave like a co-surfactant. Thus the addition of guest molecules may cause a reduction of interfacial tension and hence, decrease the size of aggregates. Nanoparticles have a very large interface because of their small droplet size. The thermodynamic stability of the aggregates can only be achieved if the interfacial tension is so low that the positive interfacial energy given by $\gamma A$ (with A = interfacial area) can be compensated by the negative free energy of mixing $\Delta G_m = -T\Delta S_m$. The entropy of mixing is the order of the Boltzmann constant

*Michał R. Radowski, Dissertation*

$k_B$; hence the limiting value of $\gamma$ required for a stable nanoparticle droplet is $\gamma = k_B T/A$. For an equal composition (constant dispersed phase, i.e., constant dispersed volume) the interfacial area is larger for small droplets and small for large droplets. The addition of compact guest molecules causes a reduction of $\gamma$ and therefore an increase of the interfacial area i.e., smaller droplet. The disturbance of the polymer packing can be observed by AFM measurements, when the addition of nimodipine led to a disruption of the organization of the nanotransporters on the HOPG surface (Figure 59). In the case of linear guest molecules the interactions with the aggregates result in the opposite behavior. The aggregates' size and CAC increases after the encapsulation of guests. Based on AFM experiments (Figure 58) the stabilization of the surface packing was observed. It can be hypothesized that linear molecules, independent of their polarity, behave as noncovalent linkers between the polymers. The tendency of congo red[377] and β-carotene[387] to self-organize into a long species allows a long-distance bridging between nanotransporters. The obtained aggregates are therefore bigger due to the internal guest molecules backbone. The increase of the aggregates size leads to a decrease of the interfacial area which results in a bigger CAC value. The schematic mechanism of the change of the aggregates size is presented in Scheme 17.



**Scheme 17.** Mechanism of the change of the aggregates' size. Aggregation of the core-multishell architectures leads to the formation of supramolecular with diameters of 30 to 50 nm. After encapsulation of compact (small) molecules, which act as co-surfactants, the aggregates size decreases to 20 – 30 nm in diameter. With the encapsulation of linear molecules the aggregates grow to diameters of 120 to 160 nm due to cross-linking by guest molecules.

Dynamic measurements of the encapsulation process revealed two separate phases of the uptake of guest molecules. The initial phase transfer (solid-liquid) was very fast and

the progress was observed in minutes. After approximately 2 to 3 h the process slowed down and an increase of the transport capacity was only observed between intervals of hours and days. It is important that no stable saturation point was observed, although after the overloading of the core-multishell architectures a precipitation of the polymer was confirmed.

The environment sensitive dye – nile red – allowed one to localize the site of binding of the guest molecules. The absorption ($\lambda_{max}$) of nile red reveals a shift towards longer wavelengths (red shift) in polar environment and a blue shift in nonpolar media.[398] Thus, changes in $\lambda_{max}$ of the encapsulated dye indicates the polarity of the nanoenvironment surrounding the guest molecules. Studies were performed by solid-liquid extraction with $PG_{10000}(-NH_2)_{0.7}(C_{18}mPEG_6)_{1.0}$ in water with the addition of 5 mg of solid nile red. The concentration of the polymer was 1.00 g l$^{-1}$ (1.43 $\times$ 10$^{-5}$ M). Samples were measured by UV/Vis after 5, 15, 60, 120, 1440 (24 h), 2880 (48 h), 7200 (120 h), and 18900 (315 h) minutes of stirring (Figure 61). Besides the expected transport capacity (absorbance) increase, the spectra revealed a smooth blue shift of $\lambda_{max}$ from 548 nm to 505 nm during the progress of encapsulation. The sample measured after 5 minutes of process revealed a symmetrical absorption band with $\lambda_{max}$ at 548 nm. This corresponds to the absorption of nile red located in poly(ethylene glycol). Within the progress of dye uptake an appearance of a second absorption band at 505 nm was observed (Figure 61 bottom). This corresponds to the absorption of nile red in nonpolar environment like in toluene or benzene. After approximately 120 minutes the intensity of the band at 505 nm overcomes the intensity of the signal at 548 nm. During the progress of encapsulation a further increase of the signal at 505 nm was observed.
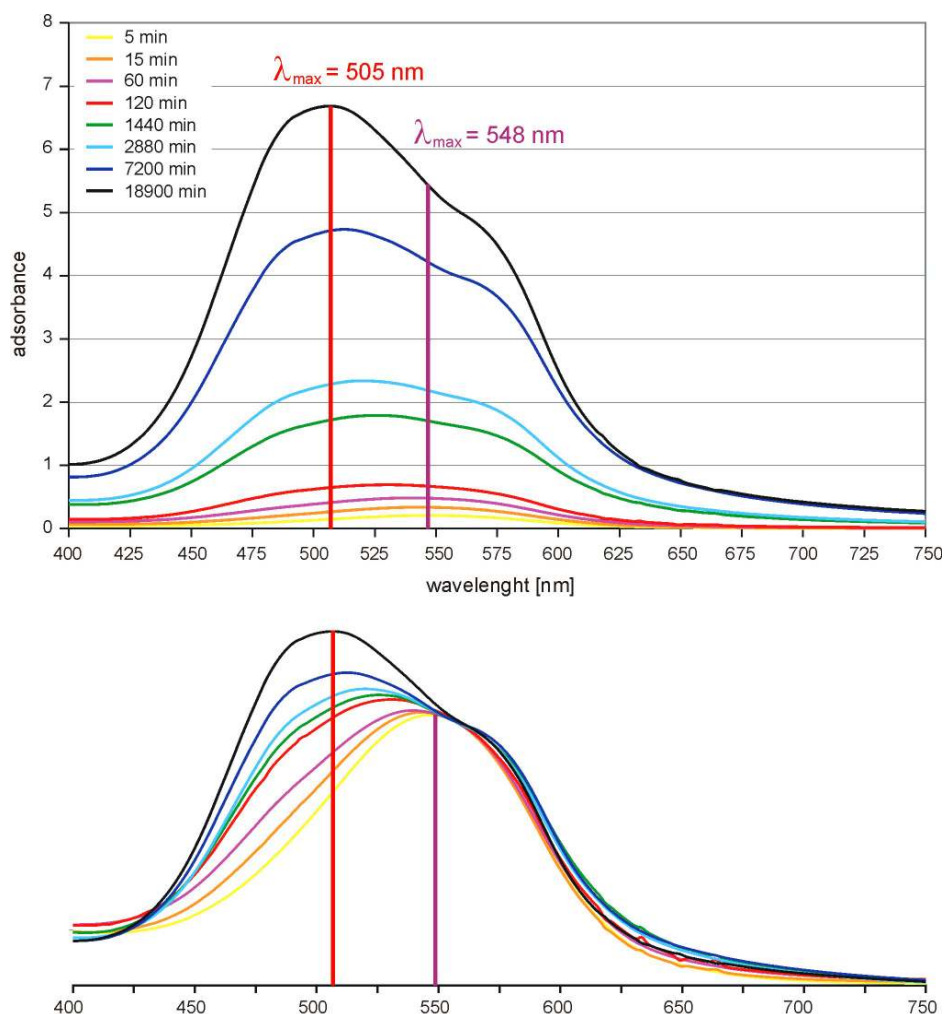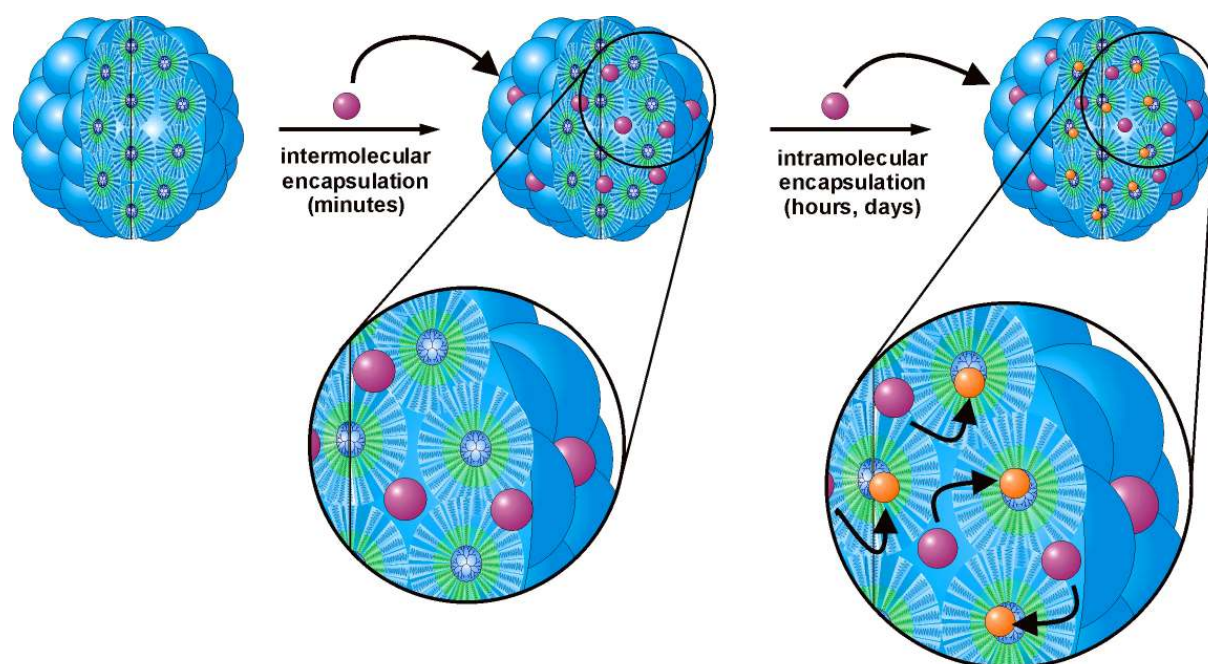
**Figure 61.** Spectra of encapsulated nile red in $PG_{10000}(-NH_2)_{0.7}(C_{18}mPEG_6)_{1.0}$ nanotransporter in water. The upper graph presents the increase of the absolute absorbance of the dye with increasing encapsulation time. Lower graph presents the spectra calibrated on the wavelength of 548 nm to visualize the increase of the intensity of the band at 505 nm in comparison to the signal at 548 nm.

The obtained results clearly indicate two different sites for the encapsulation of guest molecules. Initially, nile red is trapped between polymers in the aggregated state where a mPEG network create intermolecular cavities that are suitable for the dye (Scheme 18). This process is very fast and corresponds to the rapid increase of the transport capacity in the first 2 to 3 hours of uptake (chapter 3.4.7 and 4.3; Figure 37, 39, and 44). After a quick saturation of the intermolecular space the encapsulation process slows down but does not stop. The second period of dye uptake is based on the slow migration of guest molecules into the inner polymer cavities from the space between the unimers. Due to the presence of the aliphatic chains in the polymer structure the nanoenvironment around nile red becomes nonpolar, which explains the appearance of the new band in the UV/Vis spectra at 505 nm (corresponding to nonpolar environment). Even after 315 h of solid-liquid extraction no saturation point of the polymers was observed (Figure 44). The process of dye uptake and

*Michał R. Radowski, Dissertation*

diffusion from intermolecular into intramolecular cavities was constant in the observed time period.



**Scheme 18.** Intermolecular and intramolecular encapsulation process for core-multishell architecture.

The role of the aggregation phenomenon for transport of guest molecules can be explained as follows. The host-guest interactions first becomes possible at the intermolecular region in the aggregates, where mPEG chains create cavities which are able to encapsulate guest molecules. Also the unimers possess binding sites (cavities) that are suitable for the encapsulation of guest molecules. However, the inner cavities are not directly reachable for guests by solid-liquid extraction. Only after an initial uptake of the dyes into the intermolecular space, molecules can be further encapsulated inside the core-multishell structure (intramolecular encapsulation).

In conclusion, the self-aggregation phenomenon plays the major role for the transport abilities of core-multishell architectures. The intermolecular space with the $C_{18}$mPEG network creates suitable conditions for the extraction (dye/drug dissolution) and encapsulation of guest molecules. The flexible, dynamic structure allows the easy penetration of dyes into the aggregates. The permanent equilibrium between unimers and aggregates leads to a constant renewal of the aggregates' surface. Thus fast and efficient encapsulation is possible. After the primary encapsulation, the entrapped guest molecules are able to penetrate the polymeric structure and fill the inner cavities. This process, in contrast to the intermolecular encapsulation, can be named as intramolecular encapsulation and is exclusively dependent on the intermolecular uptake. Nevertheless it allows an increase of the transport capacity of polymers during the long encapsulation process.